

<https://doi.org/10.1038/s42005-022-01098-5>

OPEN

## The first-order structural transition in NiO at high pressure

Alexander G. Gavriluk<sup>1,2,3,7</sup>, Viktor V. Struzhkin<sup>4,7</sup>, Anna G. Ivanova<sup>1,2,7</sup>, Vitali B. Prakapenka<sup>1,2,7</sup>, Anna A. Mironovich<sup>1</sup>, Sergey N. Aksenov<sup>1</sup>, Ivan A. Troyan<sup>1,2</sup> & Wolfgang Morgenroth<sup>1,6</sup>

Insulator-metal transition in NiO and concomitant collapse of spin and magnetism in the material are important subjects in studies of strong electronic correlations and as such they generate multiple theoretical and experimental efforts aimed at understanding the complicated physics of strongly correlated electronic systems. We report here the iso-structural transition in NiO accompanying the previously observed by us transition to the metallic state. These findings resolve some experimental controversies regarding the transition. We also discuss the latest theoretical results in detail and show that our data confirm some recent theoretical models. Given the simplicity of the material and its fundamental importance to the understanding of strongly correlated electronic systems, our findings should stimulate further experimental and theoretical efforts to understand this prototype Mott insulator.

<sup>1</sup> Institute for Nuclear Research, Russian Academy of Sciences, Troitsk, Moscow 108840, Russia. <sup>2</sup> Federal Scientific Research Centre "Crystallography and Photonics" of Russian Academy of Sciences, Leninskiy Prospect, 59, 119333 Moscow, Russia. <sup>3</sup> REC «Functional Nanomaterials», Immanuel Kant Baltic Federal University, 236041 Kaliningrad, Russia. <sup>4</sup> Center for High Pressure Science and Technology Advanced Research, Shanghai 201203, China. <sup>5</sup> Center for Advanced Radiation Sources, University of Chicago, Argonne, IL 60439, USA. <sup>6</sup> Institut für Geowissenschaften Universität Potsdam, 14469 Potsdam, Germany. <sup>7</sup>These authors contributed equally: Alexander G. Gavriluk, Viktor V. Struzhkin, Anna G. Ivanova.  email: [viktor.struzhkin@hpstar.ac.cn](mailto:viktor.struzhkin@hpstar.ac.cn)

The importance of the insulator-metal transition (IMT) in compressed nickel monoxide (NiO) for the physics of strongly correlated electronic systems ranks close to the problems of insulator-metal transition and high-temperature superconductivity in cuprates and to other key problems in physics (according to Ref. <sup>1</sup>), such as metallization of hydrogen under pressure. NiO was historically the first material, which proved to be a test-bed for the understanding of strongly correlated electronic systems. In pioneering studies by Mott and co-workers, NiO was treated as a typical example of “Mott” insulator with a wide *d-d* energy gap  $E_g$ , which occurs due to strong on-site Coulomb electron repulsion between Ni 3d electrons<sup>2-5</sup>. At the same time, Mott predicted possible IMT in compressed NiO. The first suggestions of metallic high-pressure phase of NiO were made by Boer, Verwey, Mott, and Peierls<sup>6,7</sup>. Recently we observed the IMT transition in NiO at  $240 \pm 10$  GPa in experiments probing the resistance of the samples at high pressure<sup>8</sup>. Numerous theoretical studies provided contradictory predictions regarding the pressure range and nature of the IMT in NiO. Early theoretical LDA and GGA calculations by Cohen et al.<sup>9</sup> predicted that band-broadening effects are responsible for a magnetic collapse in simple oxides FeO, MnO, and CoO; a nearly second-order phase transition accompanied by magnetic collapse at 230 GPa was predicted in NiO<sup>9</sup>. In the paper by Feng et al.<sup>10</sup> it was shown that the more ‘sophisticated’ B3LYP density functional predicts a transition at significantly higher pressure than the GGA functional. More recent predictions from the ab-initio (LSDA + U) calculations performed by the authors of Ref. <sup>11</sup>, indicated a transition above 300 GPa; the most recent calculation using DMFT method predicted the transition pressure at 429 GPa in NiO<sup>12</sup> (see discussion section for further comments). Thus, the theoretical controversy regarding the pressure of the transition is not resolved by recent publications.

It should be noted here that the existing experimental claim of transition pressure exceeding 280 GPa in NiO<sup>11</sup> is based on NFS measurements at just one pressure point with the signal level about ten counts (total) in maximum, which makes it difficult to validate the claimed complicated signal pattern, relevant to the magnetic phase. Moreover, the effect of pressure gradients (which could be of the order of 30 – 40 GPa in non-hydrostatic conditions above 200 GPa) on the experimentally obtained NFS data is not given a proper discussion in<sup>11</sup>.

Given such controversial situation in the existing literature on the IMT in NiO, it is extremely important to study the NiO by independent experimental techniques. For this purpose, we have performed structural studies of NiO to elucidate possible structural changes at the transition.

Since the reported theoretical and experimental studies<sup>8,10,13-16</sup> suggest a very high pressure of the transition in NiO, we have approached this important problem using multimegarbar diamond anvil cell techniques.

The paper presents the results of structural studies of NiO in the widest possible pressure range of (0–240 GPa) to date. Starting from  $\sim 110$  GPa, we observe a significant trigonal distortion of the initially NaCl-type crystal structure. At higher pressures, a structural transition with a volume drop of  $\sim 2.7\%$  was detected experimentally in the region of the insulator-metal transition. Finally, we report here the observation of the first-order structural transition accompanying the insulator-metal transition in NiO.

## Results

We tested original NiO sample at STOE multi-purpose diffractometer system “STADI MP” and found volume and lattice parameter  $a = 4.1779(2)$  Å,  $V = 72.927(2)$  Å<sup>3</sup> for the B1 cubic phase of the NiO structure ( $Fm\bar{3}m$ ) and  $a = 2.9558(1)$  Å,  $c = 7.2283(1)$  Å,  $V_0 = 54.692(1)$  Å<sup>3</sup> for the trigonal phase ( $R\bar{3}m$ ) of the distorted

B1 structure. Corresponding X-ray data and lattice parameters are presented in Supplementary Note 1.

We have made five runs of X-ray diffraction (XRD) experiments with NiO up to 238 GPa in standard and beveled diamond anvil cells at hydrostatic and nonhydrostatic conditions at room temperature up to very high pressures (Table 1). The images of the NiO samples in diamond anvils cells from runs 1–5 are shown in Fig. 1.

The evolution of the XRD patterns taken from NiO samples in the pressure range 0–40 GPa in a quasi-hydrostatic experiment with PES-5 as a pressure medium (run1) is shown in Fig. 2(a). The evolution of the XRD patterns in the pressure range 31–73 GPa in a hydrostatic experiment with Ne as a pressure medium (run2) is shown in Fig. 2(b). The evolution of the XRD patterns in a quasi-hydrostatic experiment with Ne as a pressure medium in the pressure range 111–161 GPa (run3) is shown in Fig. 2(c). The evolution of XRD patterns in a quasi-hydrostatic experiment with NaCl as a pressure medium in the pressure range 129–238 GPa (run4) is shown in Fig. 2(d).

In the non-hydrostatic measurements (run5) the NiO sample itself was used as a pressure medium in c-BN gasket<sup>17</sup>. The image of the NiO sample in the non-hydrostatic experiment is shown in Fig. 1(e).

Recent XRD experiments on the distorted rock-salt structure of NiO have found this structure to be stable up to  $\sim 147$  GPa<sup>14</sup>. In the most recent study the absence of the transition was claimed up to 212 GPa<sup>11</sup>.

In this study we determined the experimental V-P relation of NiO at hydrostatic and quasi-hydrostatic conditions up to 238 GPa (Fig. 3). We observed (for run4 with NaCl pressure medium) an onset of an iso-structural transition with a volume drop about 2.65% (estimated at 225 GPa) during pressure increase in the region 208–238 GPa. The Birch-Murnaghan equation of state was fitted to the current experimental data, and its parameters were found to be  $B_0 = 192 \pm 7$  GPa, and  $B' = 4.8 \pm 0.1$  for the low-pressure phase (LP) below  $\sim 208$  GPa (see details in Supplementary Note 5). For the high-pressure phase (HP), we used a fit of the experimental data (measured at non-hydrostatic conditions in run5) to a modified Birch-Murnaghan equation of state (see details in Supplementary Note 5); the parameters are presented below. The solid line shown in Fig. 3 represents the calculated Birch-Murnaghan equation of state that fits well all the sets of the experimental data.

We did not find any substantial influence of the non-hydrostaticity on the P-V relation of NiO up to  $\sim 100$  GPa. At pressures higher than  $\sim 100$  GPa for non-hydrostatic measurements the influence of non-hydrostatic strain was taken into account during the fitting procedure<sup>18-20</sup>. From our fit we found that for the higher pressures (above 100 GPa) the effective value of the strain is also higher. We observed the first-order structural transition in NiO with an effective pressure of the transition about  $225 \pm 15$  GPa (see Fig. 3 and details in Supplementary Note 5).

We also observed an anomaly in the *a/c* ratio during hydrostatic compression at about 50 GPa. The anomaly is clearly seen in Fig. 4. This “kink-like” anomaly is in excellent agreement with the kink in the pressure dependence of the optical gap at  $\sim 50$  GPa (see inset in Fig. 4, and Ref. <sup>8</sup>).

The pressure evolution of XRD patterns from non-hydrostatic run5 below and at the structural transition in NiO is shown in Fig. 5. An increase in pressure above 130 GPa leads to a trigonal distortion of the cubic crystal structure. In addition, the observed splitting of the 012 reflection of the trigonal structure at  $\sim 206$  GPa clearly indicates the coexistence of the high-pressure (HP) and the low-pressure (LP) phases in the region of the structural transition. Figure 6 shows the spatial linear scans of X-ray patterns of NiO at different pressures: (a) for 208 GPa, and (b) for 133 GPa after

Name of run	Pressure region, GPa	Anvil's shape	Pressure transmitting medium	Hydrostaticity	Pressure sensors	Gasket material
Run-1	0.5-39.5	Flat, 300 $\mu\text{m}$ diameter	Silicon oil PES-5	Quasi-hydrostatic	Au <sup>42</sup>	Re
Run-2	31.1-73.4	Flat, 150 $\mu\text{m}$ diameter	Neon	hydrostatic	Au <sup>42</sup>	Re
Run-3	111.6-161.6	double-bevel, 120 $\mu\text{m}$ (7.5 deg), 240 $\mu\text{m}$ (11.5 deg), flat 25 $\mu\text{m}$	Neon	Quasi-hydrostatic	Neon <sup>42</sup>	c-BN
Run-4	129-238	single-bevel, 270 $\mu\text{m}$ diameter, 8.5 deg, flat 55 $\mu\text{m}$	NaCl	Quasi-hydrostatic	diamond scale <sup>43</sup>	Re
Run-5	95.8-224	single-bevel, 240 $\mu\text{m}$ diameter, 8.5 deg, 30 $\mu\text{m}$	c-BN	Non-hydrostatic	Au <sup>42</sup>	c-BN

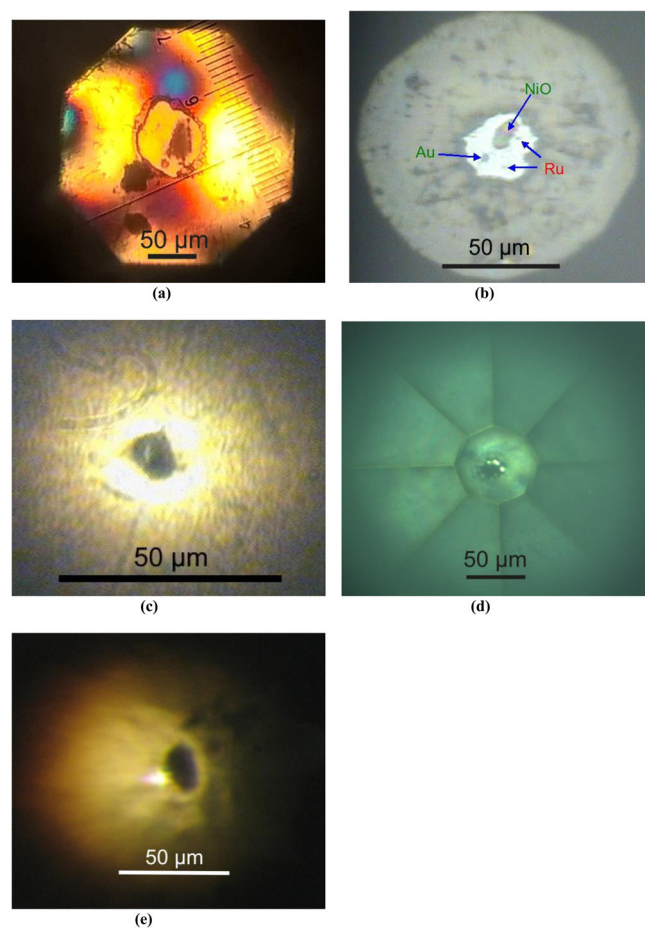


**Fig. 1 The sample loading examples.** **a** The mount of quasi-hydrostatic measurements in PES-5 pressure medium. The powdered NiO sample at P-10 GPa, and a piece of Au are placed inside the hole in the Re gasket. The pressure medium is silicon oil PES-5 (run1). **b** The mount of hydrostatic measurements in Ne pressure medium. The powdered NiO sample at P-36 GPa, piece of Au and two Ruby chips are placed inside the hole in the Re gasket. The pressure medium is neon (run2). **c** The mount of hydrostatic measurements in Ne pressure medium with a cBN gasket. The powdered NiO sample at P- 110 GPa are placed inside the hole in the cBN gasket. The pressure medium is neon (run3). **d** The mount of quasi-hydrostatic measurements in NaCl pressure medium with Re gasket. The powdered NiO sample at P- 208 GPa are placed inside the hole in the Re gasket. The pressure medium is NaCl (run4). **e** The image of the experimental mount of non-hydrostatic measurements. The powdered NiO sample at ~209 GPa completely fills the hole in the central part of the cBN gasket. At the edge of cullet a small piece of gold, which was used as a pressure sensor. The cullet has oval shape with dimensions ~25  $\times$  30  $\mu\text{m}$  (run5).

decompression. It is important to note here, that the pressure during the spatial scan across the phase boundary was constant. Taking into account the small beam spot size ( $2 \times 4 \mu\text{m}^2$ ) we believe that the observed splitting of 012 reflection is caused by the coexistence of two different phases and is not related to the pressure gradient. We clearly observe a decrease of the intensity of reflections corresponding to the HP phase and consequent increase of LP reflections intensity when crossing the phase boundary (see Fig. 6). We show the V-P relation of NiO measured in nonhydrostatic experiment (run5) in Fig. 7. The unit cell volume decreases gradually with pressure increase. At ~210–220 GPa we observed a first-order iso-structural transition, which was accompanied by the volume drop of about 2.7%. The difference between the observed pressure values of the structural and the IMT<sup>8</sup> phase transitions can

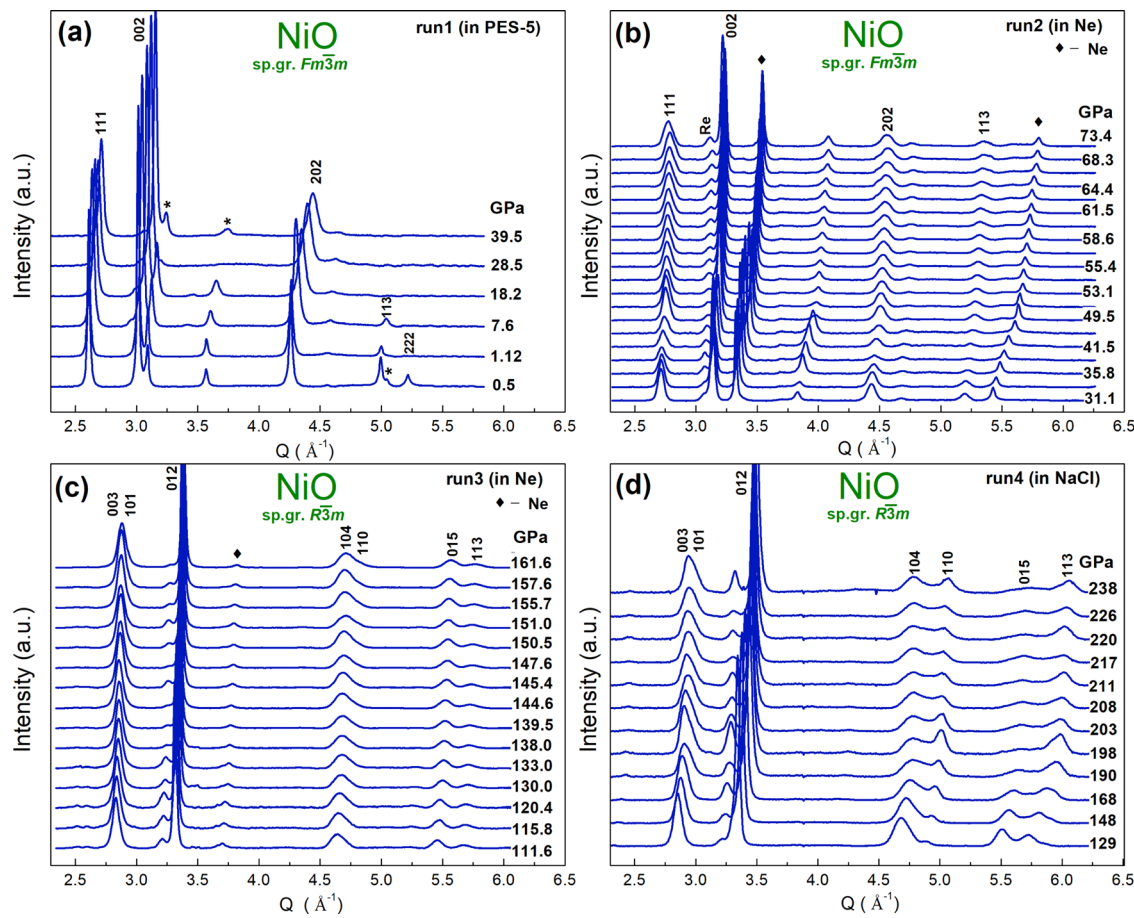


**Fig. 2 The evolution of the X-ray diffraction (XRD) patterns of NiO with pressure increase at room temperature for different runs.** **a** XRD patterns of run 1 (impurity peaks of Ni are marked with asterisks), **(b)** XRD patterns of run 2, **(c)** XRD patterns of run 3, **(d)** XRD patterns of run 4.

be explained by overestimating the pressure of the resistive IMT and underestimating the pressure of the isostructural transition in the X-ray measurements. The overestimation is due to the specificity of the mechanism of formation of the conducting region in the sample through percolation and the underestimation of the transition pressure in the XRD measurements is caused by the pressure drop just after the phase transition. The careful considerations and detailed analysis of the exact pressure value of the structural transition is presented in the Supplementary Note 4.

In summary, from this analysis, we estimate the pressure value of the transition to be around  $\sim 225 \pm 15$  GPa. The Birch-Murnaghan equation of state was fitted to current experimental data, and its parameters were found as  $B_{LP0} = 216 \pm 15$  GPa,  $B_{LP}' = 4.3 \pm 0.4$  for low-pressure phase (LP) below  $\sim 210$  GPa. For better comparison of LP an HP phases we performed the calculations with respect to 130 GPa and obtained the following parameters for the modified BM equation of state (see in the Supplementary Note 5) of LP phase:  $(V/V_0)_{130} \sim 0.735$ ,  $B_{130} = 693 \pm 5$  GPa,  $B'_{130} = 4$  (fixed). Comparison with parameters for modified BM EOS for HP phase:  $(V/V_0)_{130} \sim 0.717$ ,  $B_{130} = 699 \pm 7$  GPa,  $B'_{130} = 4$  (fixed). Here  $V_0$ —cell volume of initial NiO at ambient conditions.

## Discussion

In summary, the structure of nickel monoxide NiO was investigated in a set of experiments at high pressures at room temperature. Different pressure media were used with different level of hydrostaticity. A first-order isostructural transition in NiO was discovered at  $225 \pm 15$  GPa.

The non-hydrostatic run5 provides very important information on the isostructural phase transition. Special attention should be paid to a careful and detailed consideration of this measurement. The experimental conditions of run5 agree mostly with the experimental conditions in our previous resistance measurements<sup>8</sup>, when IMT transition was observed. All these effects (Figs. 5 and 6) present strong evidence of the existence of the first-order structural transition in NiO in the pressure region above  $\sim 210$  GPa.

We believe it is important to discuss several aspects of the theory and we provide such discussion below. Several preceding theoretical studies have tackled the problem of pressure effects on electronic correlations in simple oxides. Recent dynamical mean field theory calculations (DMFT) of MnO by Kunes et al.<sup>21</sup> have demonstrated the importance of the spin-crossover effects induced by the increasing crystal field effects which overcome Hund's exchange energy under pressure. Notably, it follows that the effective Hubbard energy ( $U_{eff}$ ) may be strongly dependent on pressure, which is at odds with the predominant practice of considering  $U_{eff}$  as nearly pressure independent parameter<sup>15</sup>. Pressure-dependent  $U$  values have been derived by Ovchinnikov<sup>22,23</sup> within a simple theoretical framework which takes into account crystal field effects. This approach has been supported by extensive experimental results for Fe-based oxide materials<sup>23,24</sup>. However, for a  $d^8$  configuration (a case for NiO) very little change in Hubbard energy is expected during compression<sup>23</sup>. It has been suggested that the Mott-Hubbard  $d-d$  energy  $U$  in NiO is comparable in magnitude to the  $p-d$  charge transfer energy  $\Delta$ <sup>25,26</sup>, and NiO is situated on the borderline between Mott insulator and charge transfer insulator regimes. However, recent resonant inelastic scattering experiments<sup>27</sup> indicate that the lowest energy gap  $E_g$  in

NiO is related to the  $d$ - $d$  charge transfer process between neighboring Ni sites strongly hybridized with the  $p$ - $d$  charge transfer. The same authors claim that their result is compatible with LDA + U model having effective Hubbard U = 8 eV.

In the most recent theoretical study by the DMFT method, Leonov et al.<sup>12</sup> have found transition pressure about 429 GPa for

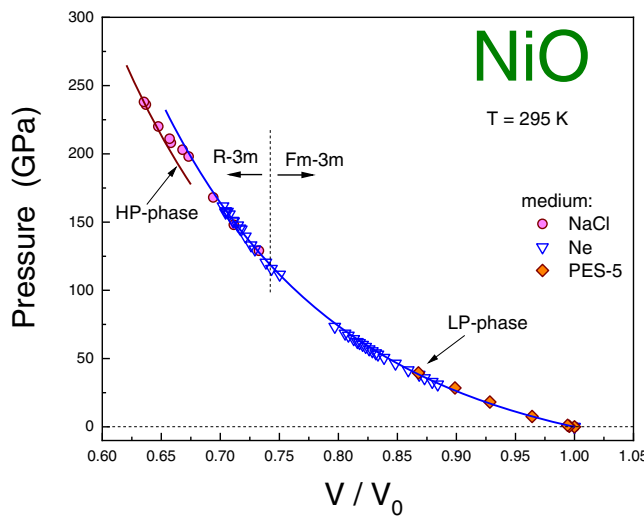


**Fig. 3 The experimental pressure-volume dependence in NiO at hydrostatic and quasi-hydrostatic conditions up to 238 GPa.** The figure combines values of relative volume change  $V/V_0$  obtained from different high-pressure experiments. The diamonds correspond to run1, triangles correspond to run2 and run3, and circles correspond to run4. As pressure increased in the range of 208–238 GPa (run4), the onset of the isostructural transition was observed with a volume drop about 2.65%. The Birch-Murnaghan equation of state was fit to current experimental data, and its parameters were found are equal to  $B_0 = 192 \pm 7$  GPa,  $B' = 4.8 \pm 0.1$  for low-pressure phase (LP) below ~208 GPa (in blue). For high-pressure phase (HP) we used fit of nonhydrostatic experimental data for modified Birch-Murnaghan equation of state (Supplementary Note 5). The solid line—calculated Birch-Murnaghan equations of state fit very well all sets of experimental points including.

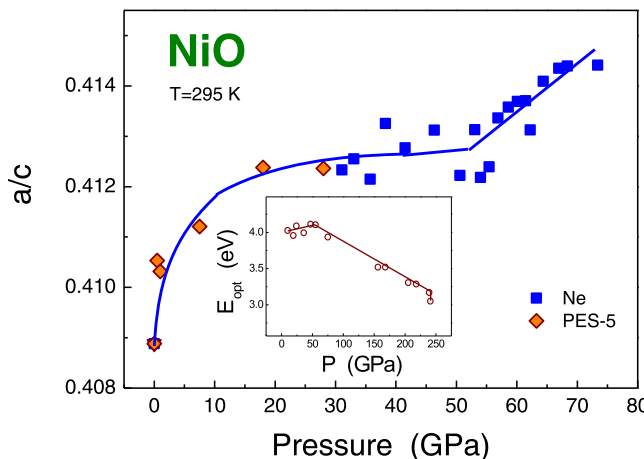


**Fig. 4 The pressure dependence of the lattice constant ratio for NiO in hydrostatic and quasi-hydrostatic experiments at room temperature.** The values of lattice constant ratio  $a/c$  calculated from X-ray diffraction for NiO in hydrostatic (run2) and quasi-hydrostatic (run1) experiments are shown in blue squares and orange diamonds. There is a kink at ~55 GPa which is related to the kink in the pressure dependence of the optical gap (shown in inset)<sup>8</sup>.

NiO, using  $U = 10$  eV,  $J = 1$  eV. However, they also point to significant reduction of the calculated transition pressure (to 248 GPa), if they use  $U = 8$  eV,  $J = 1$  eV instead. In their paper, they give a long list of references, which actually includes nearly 30 papers, to justify their choice of parameters  $U$  and  $J$ . However, going through that list of papers, we find very different suggested parameters, especially Hubbard  $U$  has quite a broad range from 7 to 10 eV in NiO. For example, the modeling of XAS spectra gives it as low as  $U = 7.6$  eV<sup>28</sup>. It should be noted that since Leonov et al.<sup>12</sup> give no further arguments in support of their choice of  $U = 10$  eV for NiO, the very high predicted transition pressure for NiO is not reliable, given the fact that even their calculations produce transition pressure about 248 GPa for  $U = 8$  eV, which is much closer to the experimentally reported pressure of IMT<sup>8</sup> and to the reported values of the Hubbard  $U$  as discussed below. The resonant inelastic scattering experiments in NiO at ambient pressure<sup>27</sup> provided Hubbard  $U = 8$  eV. The high-pressure studies of the resonant inelastic scattering in NiO<sup>29</sup> show that ~8 eV feature is almost independent on pressure and broadens dramatically above 60 GPa. Given all this experimental evidence, it is difficult to accept the value  $U = 10$  eV as suggested by Leonov et al.<sup>12</sup>. As outlined above, our values of transition pressures from the XRD measurements and from the IMT<sup>8</sup> transition confirm the recent theoretical studies by Leonov et al.<sup>12</sup> by DMFT calculations with transition pressure about 248 GPa for NiO, using  $U = 8$  eV,  $J = 1$  eV.

In addition, we observed (run5) the coexistence of high- and low-pressure phases in the wide pressure range during decompression from ~230 to ~130 GPa. We also note that we observed a spatial separation of regions of pure high- and low-pressure phases at the same pressure values. The volume drop of about 2.65 % was observed in quasi-hydrostatic conditions, while in non-hydrostatic conditions the volume drop was about 2.7%. The observed structural transition is in a good agreement with the insulator-metal transition observed at 240 GPa in NiO recently<sup>8</sup>. It is generally believed that the structural transition is a result of Mott-type IMT transition<sup>8</sup> which occurs when the effective Hubbard parameter is nearly equal to the total  $d^8$  bandwidth, or  $U_{\text{eff}} \sim 2$  W. Notably, the high-pressure phase was observed during decompression down to ~130 GPa. We found a stratification of the sample into regions of pure high- and low-pressure phases at the same pressure value. It is

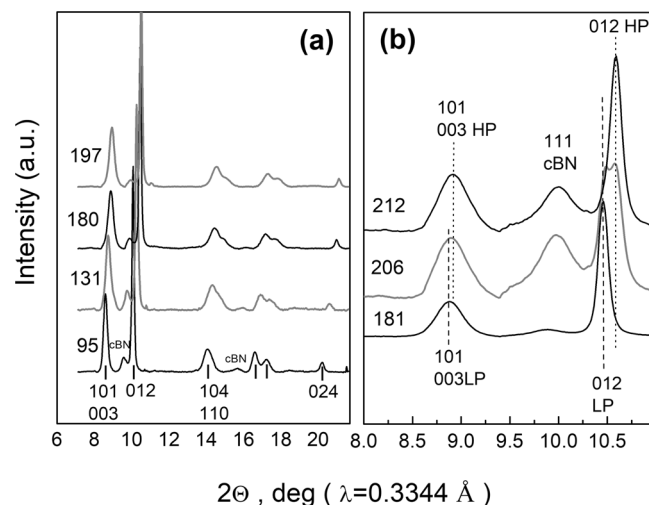


**Fig. 5 The X-ray diffraction patterns of NiO in non-hydrostatic experiment in the megabar pressure range.** **a** The evolution of X-ray diffraction (XRD) patterns of NiO in run5 with pressure increase below the structural transition. **b** The evolution of XRD patterns of NiO in run5 with pressure increase in the region of structural transition (181–212 GPa).

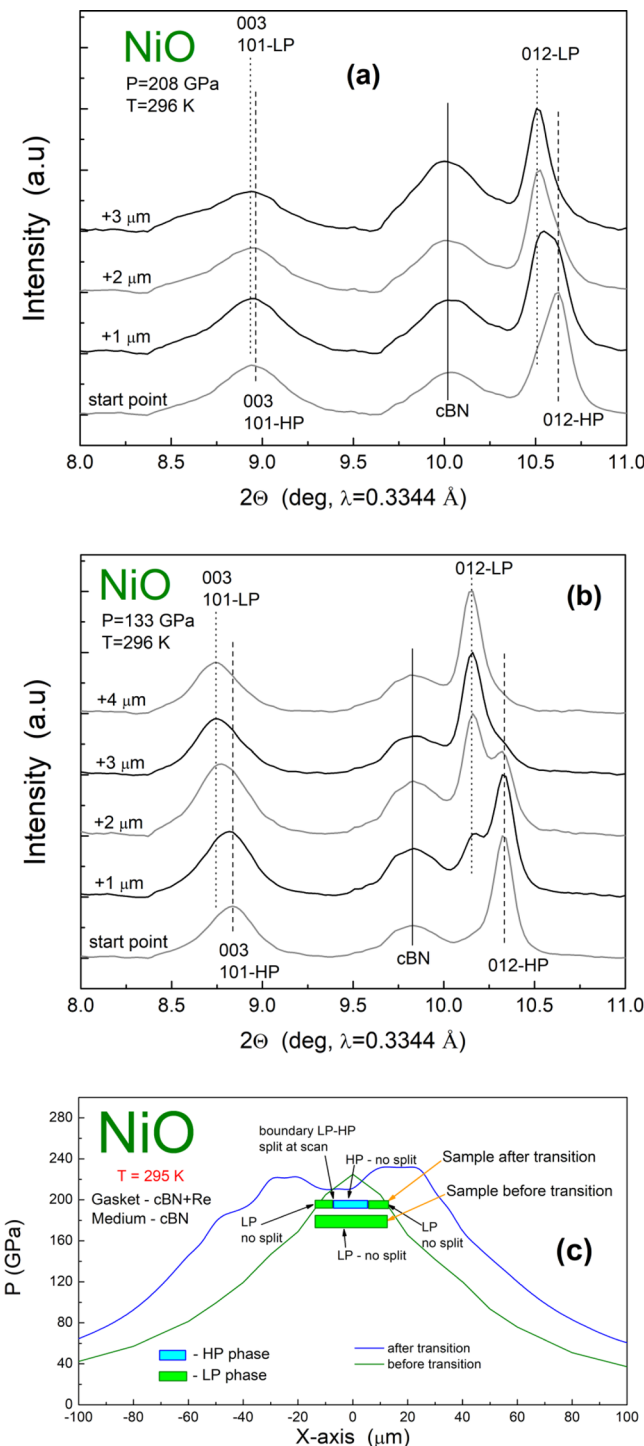


**Fig. 6 The evolution of X-ray diffraction patterns along the NiO sample in a non-hydrostatic experiment at different pressures.** **a** X-ray diffraction (XRD) patterns collected in the linear scan along the x-axis with a step of  $1\mu\text{m}$  at  $208$  GPa (run5), **(b)** XRD patterns collected in the same scan at  $133$  GPa after decompression (run5) (Supplementary Note 3). We clearly observed the splitting of the reflections corresponding to simultaneous measurements of high-pressure (HP) and low-pressure (LP) structures. There is stratification resulting in some regions of pure high- and low-pressure phases at the same pressure value. The scan line crosses the boundary between these two phases. The illustration of stratification of LP and HP phases is shown in panel **(c)**.

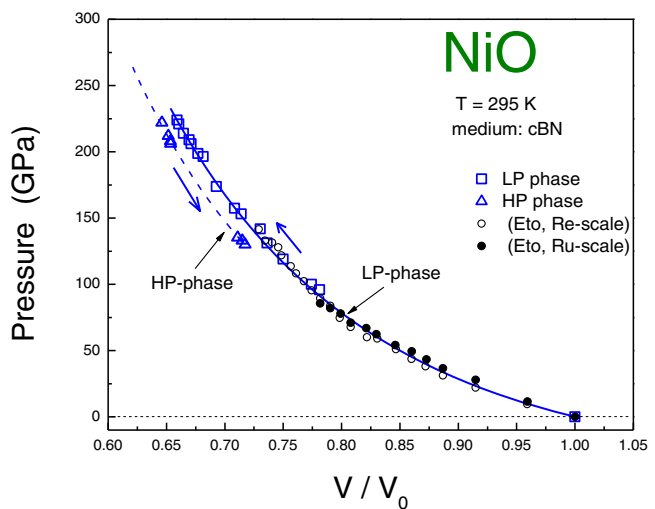


**Fig. 7 The experimental relation pressure-volume dependence in NiO at non-hydrostatic conditions.** The figure combines values of the relative volume change  $V/V_0$  obtained from our nonhydrostatic experiment (run5) and from Eto's et al work (Ref. 14). The open triangles correspond to high-pressure phase (HP). For comparison are shown previous experimental data from Eto's et al. work (Ref. 14)—circles (open circles—Re calibrated pressure, closed circles—Ruby calibrated pressure). The Birch-Murnaghan equation of state was fitted to the experimental data (run5), and its parameters were found are equal the bulk modulus  $B_0 = 216 \pm 15$  GPa and its derivative  $B' = 4.3 \pm 0.4$ . The solid line—calculated Birch-Murnaghan equation of state fits very well all set of experimental points including previous one (Ref. 14). With a pressure increase in the range of  $206$ – $224$  GPa the onset of the isostructural transition was observed with a volume drop of about 2.7%. In our non-hydrostatic experiment (run5) we observed a coexistence of high- and low-pressure phases in a wide pressure interval from  $\sim 230$  to  $\sim 130$  GPa at decompression. For the HP phase, we used fit of non-hydrostatic experimental data for the modified Birch-Murnaghan equation of state (Supplementary Note 5) and its parameters were found are equal to bulk modulus  $B_{130} = 699 \pm 6$  GPa its derivative  $B_{130}' = 4.0$  (fixed) with initial pressure parameter of  $130$  GPa.

known that the nanometer scale inhomogeneous regions in transition metal oxides are strongly linked to such phenomena as colossal magnetoresistance, and to the coexistence of several interactions between spin, charge, lattice, and orbital degrees of freedom, such as observed in cuprates<sup>30</sup>.

We would like to point out here that to our knowledge the electronic transitions in oxides at high pressures are accompanied in most cases by volume discontinuities and sometimes with very pronounced changes in the crystal structure. For example,  $\text{MnO}$  is another example of a transition metal oxide having isostructural electronic transition around  $\sim 105$  GPa with 6.6% volume collapse (claimed to be a Mott transition), showing coexisting phases around the transition—see Fig. 5 in Ref. 31, and also “considerable” hysteresis effects on the release of pressure as claimed in the Ref. 32. Moreover, considering other types of electronic transitions, we observed such extreme cases as electronic spin transition accompanied with a structural change to amorphous phase recoverable to ambient pressure in  $\text{YIG}$  crystals<sup>33</sup>. Another example is electronic spin transition in  $\text{NdFeO}_3$  around  $40$  GPa having both volume collapse and significant hysteresis<sup>34</sup>. We can additionally give the example of the pressure-induced first-order isostructural Mott insulator-metal transition in cubic  $\text{PbCrO}_3$ , accompanied by a sharp volume collapse which has been interpreted in terms of charge

**Table 2** The details of experimental set-ups and other technical aspects of XRD experiments with NiO at high-pressure.

Name of run	Set-Up	Wavelength, Å	Detector	Beam size	Distance
Run-1	ID27 (ESRF)	0.3738 Å	MAR CCD 165	~2 × 3 μm <sup>2</sup>	216 mm
Run-2	GSECARS 13ID (APS)	0.3344 Å	MAR165 CCD	~3 × 3 μm <sup>2</sup>	203 mm
Run-3	GSECARS 13ID (APS)	0.3344 Å	MAR165 CCD	~3 × 3 μm <sup>2</sup>	203 mm
Run-4	P02.2 (PETRA III)	0.2945 Å	Perkin Elmer (XRD 1621)	~2 × 2.2 μm <sup>2</sup>	491 mm
Run-5	GSECARS 13ID (APS)	0.3344 Å	MAR165 CCD	~3 × 3 μm <sup>2</sup>	202 mm

disproportionation in the low-pressure insulating phase<sup>35–37</sup>. These are not the only examples of the concomitant changes in the crystal structure at the electronic transition in transition metal oxides, however, it is extremely difficult to find an example of “pure” isostructural electronic transition without volume discontinuity in oxides at high pressures. Thus, the hysteresis effects will vary from system to system and are very sensitive to pressure environment. Given the above examples, the behavior of NiO under pressure is not unusual. The “huge” nearly 100 GPa hysteresis in NiO in non-hydrostatic settings is remarkable, and future experiments may help to understand such behavior. Furthermore, the drop in pressure at the central part of the transformed sample is expected since after transition has happened, the volume of the sample in the central part has decreased and there is not enough plasticity in the sample to compensate this decrease by the flow of the material towards the center of the sample.

The spatial scale of regions of HP and LP phases in NiO is not identified at the moment, but the dimensions of the separated phases must be quite large according to the observed relatively narrow X-ray diffraction peaks. To understand the effects of stress on the phase separation, future studies should address the whole pressure interval of the coexistence of the HP and the LP phases in NiO in more hydrostatic pressure media to clarify the hysteresis effects of the reverse transition. Given the simplicity of the material and its fundamental importance to the understanding of strongly correlated electronic systems, our findings should stimulate further experimental and theoretical studies of NiO, a prototype Mott insulator.

## Methods

We used standard NiO powder supplied by “Alpha Aesar” company for sample preparation.

To perform XRD experiments under high pressure in five runs 1–5, NiO samples were loaded in five DACs<sup>38</sup> with standard and beveled diamond anvils with different pressure transmitting media (Table 1 and Fig. 1). The detailed characteristics of synchrotron XRD experiments with NiO under high-pressure are presented in Table 2. Linear XRD scans through the NiO sample in run5 were made with 1 μm step. The powder XRD images were integrated to one-dimensional patterns using the FIT2D<sup>39</sup> and DIOPTAS software<sup>40</sup>. The whole profile analysis of the diffraction data and the calculation of the unit cell parameters were performed in JANA200 program<sup>41</sup> using the Le Bail method.

## Data availability

All data are available in the main text, the supplementary information or sends a request corresponding author (viktor.struzhkin@hpstar.ac.cn) or to AGG (gavriliuk@mail.ru).

Received: 11 November 2021; Accepted: 21 November 2022;

Published online: 30 January 2023

## References

1. Ginzburg, V. L. What problems of physics and astrophysics seem now to be especially important and interesting (thirty years later, already on the verge of XXI century)? *Phys. Usp.* **42**, 353–373 (1999).
2. Austin, I. G. & Mott, N. F. Metallic and Nonmetallic Behavior in Transition Metal Oxides. *Science* **168**, 7177 (1970).
3. Mott, N. F. The Basis of the Electron Theory of Metals, with Special Reference to the Transition Metals. *Proc. Phys. Soc. Sect. A* **62**, 416 (1949).
4. Mott, N. F. On the transition to metallic conduction in semiconductors. *Can. J. Phys.* **34**, 1356–1368 (1956).
5. Mott N. F. *Metal-insulator Transitions*. Taylor and Francis (1990).
6. de Boer, H. J. & Verwey, E. J. W. Semi-conductors with partially and with completely filled 3d-lattice bands. *Proc. Phys. Soc.* **49**, 59 (1937).
7. Mott, N. F. & Peierls, R. Discussion of the paper by de Boer and Verwey. *Proc. Phys. Soc.* **49**, 72 (1937).
8. Gavriliuk, A. G., Trojan, I. A. & Struzhkin, V. V. Insulator-Metal Transition in Highly Compressed NiO. *Phys. Rev. Lett.* **109**, 086402 (2012).
9. Cohen, R. E., Mazin, I. I. & Isaak, D. G. Magnetic Collapse in Transition Metal Oxides at High Pressure: Implications for the Earth. *Science* **275**, 654 (1997).
10. Feng, X.-B. & Harrison, N. M. Metal-insulator and magnetic transition of NiO at high pressures. *Phys. Rev. B* **69**, 035114 (2004).
11. Potapkin, V. et al. Magnetic interactions in NiO at ultrahigh pressure. *Phys. Rev. B* **93**, 201110(R) (2016).
12. Leonov, I., Shorikov, A. O., Anisimov, V. I. & Abrikosov, I. A. Emergence of quantum critical charge and spin-state fluctuations near the pressure-induced Mott transition in MnO, FeO, CoO, and NiO. *Phys. Rev. B* **101**, 245144 (2020).
13. Gavriluk, A. G., Troyan, I. A., Lyubutin, I. S. & Sidorov, V. A. The Effect of High Pressure on the Structure and on the Magnetic and Electronic Properties of Nickel Monoxide. *JETP* **92**, 696–697 (2001).
14. Eto, T., Endo, S., Imai, M., Katayama, Y. & Kikegawa, T. Crystal structure of NiO under high pressure. *Phys. Rev. B* **61**, 14984 (2000).
15. Massey, M. J., Chen, N. H., Allen, J. W. & Merlin, R. *Phys. Rev. B* **42**, 8776 (1990).
16. Sidorov, V. A. Differential thermal analysis of magnetic transitions at high pressure: Néel temperature of NiO up to 8 GPa. *Appl. Phys. Lett.* **72**, 2174 (1998).
17. Funamori, N. & Sato, T. A cubic boron nitride gasket for diamond-anvil experiments. *Rev. Sci. Instr.* **79**, 053903 (2008).
18. Kantor, A. et al. High-pressure structural studies of eskolaite by means of single-crystal X-ray diffraction. *Am. Mineralogist* **97**, 1764–1770 (2012).
19. Singh, A. K., Balasingh, C., Mao, H.-K., Hemley, R. J. & Shu, J. Analysis of lattice strains measured under nonhydrostatic pressure. *Jour Appl Phys.* **83**, 7567 (1998).
20. Shieh, S. R., Duffy, T. S. & Shen, G. Elasticity and strength of calcium silicate perovskite at lower mantle pressures. *Phys. Earth Planet. Inter.* **93**, 143–144 (2004).
21. Kuneš, J., Lukyanov, A. V., Anisimov, V. I., Scalettar, R. T. & Picket, W. E. Collapse of magnetic moment drives the Mott transition in MnO. *Nat. Mater.* **7**, 198–202 (2008).
22. Ovchinnikov, S. G. Spin-crossover influence on the Mott-Hubbard transitions at high pressures. *JETP* **134**, 140–146 (2008).
23. Lyubutin, I. S., Ovchinnikov, S. G., Gavriliuk, A. G. & Struzhkin, V. V. Spin-crossover-induced Mott transition and the other scenarios of metallization in 3d<sup>n</sup> metal compounds. *Phys. Rev. B* **79**, 085125 (2009).
24. Gavriliuk, A. G. et al. Another mechanism for the insulator-metal transition observed in Mott insulators. *Phys. Rev. B* **77**, 155112 (2008).
25. Zaanen, J., Sawatzky, G. A. & Allen, J. W. Band Gaps and Electronic Structure of Transition-Metal Compounds. *Phys. Rev. Lett.* **55**, 418 (1985).
26. Anisimov, V. I., Zaanen, J. & Andersen, O. K. *Phys. Rev. B* **44**, 943 (1991).
27. Hiraoka, N. et al. Charge transfer and dd excitations in transition metal oxides. *Eur. Phys. J. B* **70**, 157–162 (2009).
28. Gouguassis, C. et al. Intrinsic charge transfer gap in NiO from Ni K-edge x-ray absorption spectroscopy. *Phys. Rev. B* **79**, 045118 (2009).
29. Shukla, A. et al. Charge transfer at very high pressure in NiO. *Phys. Rev. B* **67**, 081101 (2003).
30. Dagotto, E. Complexity in Strongly Correlated Electronic Systems. *Science* **309**, 257–262 (2005).
31. Yoo, C. S. et al. First-Order Isostructural Mott Transition in Highly Compressed MnO. *Phys. Rev. Lett.* **94**, 115502 (2005).
32. Yagi, T., Kondo, T. & Syono, Y. High pressure in situ X-ray diffraction study of MnO to 137 GPa and comparison with shock compression experiment. *AIP Conf. Proc.* **429**, 159 (1998).

33. Gavriluk, A. G. et al. Equation of State and High-Pressure Irreversible Amorphization in  $Y_3Fe_5O_{12}$ . *JETP Lett.* **83**, 37–41 (2006).
34. Gavriluk, A. G. et al. Electronic and Structural Transitions in  $NdFeO_3$  Orthoferrite under High Pressures. *JETP Lett.* **77**, 619–624 (2003).
35. Xiao, W., Tan, D., Xiong, X., Liu, J. & Xu, J. Large volume collapse observed in the phase transition in cubic  $PbCrO_3$  perovskite. *PNAS* **107**, 14026–14029 (2010).
36. Wang, S. et al. Unusual Mott transition in multiferroic  $PbCrO_3$ . *PNAS* **112**, 15320–15325 (2015).
37. Cheng, J. et al. Charge disproportionation and the pressure-induced insulator–metal transition in cubic perovskite  $PbCrO_3$ . *PNAS* **112**, 1670–1674 (2015).
38. Gavriluk, A. G., Mironovich, A. A. & Struzhkin, V. V. Miniature diamond anvil cell for broad range of high pressure measurements. *Rev. Sci. Instr.* **80**, 043906 (2009).
39. Hammersley A. P. FIT2D: an Introduction and Overview. In: *ESRF Internal Report ESRF97HA02T* (1997).
40. Prescher, C. & Prakapenka, V. B. DIOPTAS: a program for reduction of two-dimensional X-ray diffraction data and data exploration. *High. Press. Res.* **35**, 223 (2015).
41. Petříček, V., Dušek, M. & Palatinus, L. Crystallographic Computing System JANA2006: General features. *Z. f.ür. Kristallographie—Crystalline Mater.* **229**, 345 (2014).
42. Fei, Y. et al. Toward an internally consistent pressure scale. *Proc. Natl Acad. Sci. USA* **104**, 9182–9186 (2007).
43. Akahama, Y. & Kawamura, H. Pressure calibration of diamond anvil Raman gauge to 310 GPa. *J. Appl Phys.* **100**, 043516 (2006).

## Acknowledgements

This work was performed under support of RSF grant # 21-12-00344. The adjustment system of the Raman installation was created with the support of the Ministry of Science and Higher Education as part of the work under grant #075-15-2021-1362. During the sample loading, facilities of the Center for Collective Use “Accelerator Center for Neutron Research of the Structure of Substance and Nuclear Medicine” of the INR RAS were used. The parts of the experiments (run 1) were performed on beamline ID27 at the European Synchrotron Radiation Facility (ESRF), Grenoble, France. We are grateful to Dr. Mohamed Mezouar and Volodymyr Svitlyk at the ESRF for assistance in using beamline ID27. Portions of this work (run 2, run 3, run 5) were performed at GeoSoilEnviroCARS (The University of Chicago, Sector 13), Advanced Photon Source (APS), Argonne National Laboratory. GeoSoilEnviroCARS is supported by the National Science Foundation—Earth Sciences (EAR – 1634415) and Department of Energy- GeoSciences (DE-FG02-94ER14466). This research used resources of the Advanced Photon Source, a U.S. Department of Energy (DOE) Office of Science User Facility operated for the DOE Office of Science by Argonne National Laboratory under Contract No. DE-AC02-06CH11357. We acknowledge DESY (Hamburg,

Germany), a member of the Helmholtz Association HGF, for the provision of experimental facilities. Parts of this research (run 4) were carried out at PETRA III and we would like to thank Dr. Hanns-Peter Liermann for assistance in using P02.2.

## Author contributions

Prepare and carry out experiments, treat data, write the paper: A.G.G., V.V.S., A.G.I. Perform experiments, discuss and edit the paper: V.B.P., S.N.A., W.M. Perform data analysis, discuss and edit the paper: A.A.M. Prepare experiments, discuss and edit the paper: I.A.T.

## Competing interests

The authors declare no competing interests.

## Additional information

**Supplementary information** The online version contains supplementary material available at <https://doi.org/10.1038/s42005-022-01098-5>.

**Correspondence** and requests for materials should be addressed to Viktor V. Struzhkin.

**Peer review information** *Communications Physics* thanks the anonymous reviewers for their contribution to the peer review of this work.

**Reprints and permission information** is available at <http://www.nature.com/reprints>

**Publisher's note** Springer Nature remains neutral with regard to jurisdictional claims in published maps and institutional affiliations.



**Open Access** This article is licensed under a Creative Commons Attribution 4.0 International License, which permits use, sharing, adaptation, distribution and reproduction in any medium or format, as long as you give appropriate credit to the original author(s) and the source, provide a link to the Creative Commons license, and indicate if changes were made. The images or other third party material in this article are included in the article's Creative Commons license, unless indicated otherwise in a credit line to the material. If material is not included in the article's Creative Commons license and your intended use is not permitted by statutory regulation or exceeds the permitted use, you will need to obtain permission directly from the copyright holder. To view a copy of this license, visit <http://creativecommons.org/licenses/by/4.0/>.

© The Author(s) 2023